Persistent-random-walk approach to anomalous transport of self-propelled particles

Zeinab Sadjadi,* M. Reza Shaebani,† Heiko Rieger, and Ludger Santen
Department of Theoretical Physics, Saarland University, D-66041 Saarbrücken, Germany
(Received 12 October 2014; revised manuscript received 22 May 2015; published 25 June 2015)

The motion of self-propelled particles is modeled as a persistent random walk. An analytical framework is developed that allows the derivation of exact expressions for the time evolution of arbitrary moments of the persistent walk's displacement. It is shown that the interplay of step length and turning angle distributions and self-propulsion produces various signs of anomalous diffusion at short time scales and asymptotically a normal diffusion behavior with a broad range of diffusion coefficients. The crossover from the anomalous short-time behavior to the asymptotic diffusion regime is studied and the parameter dependencies of the crossover time are discussed. Higher moments of the displacement distribution are calculated and analytical expressions for the time evolution of the skewness and the kurtosis of the distribution are presented.

DOI: 10.1103/PhysRevE.91.062715 PACS number(s): 87.16.Uv, 05.40.−a, 87.16.Ka, 87.16.Nn

I. INTRODUCTION

Self-propelled particles undergo active Brownian motion by consuming energy, obtained either from internal or external sources. Examples range from the transport of motor proteins on cytoskeletal filaments [1], which is a biologically relevant system, to the motion of self-motile colloidal particles [2] as a nonliving realization. The particles are powered by the hydrolysis of ATP in the former case, whereas they use a chemical reaction catalyzed on their surface to swim in the latter example. The directed propulsion subject to fluctuations has been described by persistent random walks [2–4], where a tendency to move along the previous direction is taken into account. A strong self-propulsion overcomes the stochastic fluctuations and directs the motion, which renders it ballistic for short time scales [2,4]. Nevertheless, the interplay between self-propulsion and random motion in general may lead to various scenarios of anomalous diffusive dynamics on varying time scales [4]. The influence of self-propulsion diminishes over time and, eventually, a crossover to an asymptotic diffusive regime occurs.

Even in the absence of self-propulsion, the stochastic motion of particle may remain complicated because, in general, a random walker can perform steps with arbitrary turning angles and variable step lengths. Moreover, there can be a relation between the step size and the turning angle of each step. Generalized random walks had been studied, e.g., in the context of animal and cell movements as a Markovian process [5,6], i.e., by considering the motion as a series of independent draws from the step-length and turning-angle distributions for each step. While the focus of prior studies has been more on the asymptotic diffusion coefficient of such random walks, the short-time behavior is neither thoroughly investigated nor completely understood.

In the persistent-random-walk model that we study here a particle moves straight in continuous space in a randomly chosen direction over a randomly chosen distance and then changes direction by a randomly chosen turning angle. The typical trajectories of the random walker depend strongly on the chosen turning angle and distance distributions. For small values of the angular change the new direction will be strongly correlated with the old direction, introducing a directional memory into the model without changing the Markov property of the process. The emerging intermittent directional bias is controlled by the characteristics (mean, width, asymmetry, etc.) of the turning angle distribution and the probability with which the direction is unchanged, i.e. the processivity. The bias decays with time after a few turns and the directions of the particle motion become asymptotically randomized.

Memory effects have also been included in other random-walk models. In fractional Brownian motion [7], sub- or superdiffusive motion is observed asymptotically. In continuous-time random-walk (CTRW) models [8], for example, true non-Markovian effects can be implemented via broad waiting time distributions which lead to a subdiffusive dynamics of the walker. Although these approaches are conceptually very exciting, a direct comparison to experimental results is sometimes difficult. In case of intracellular transport, for example, spatial confinement as well as a finite observation time imply that the asymptotic behavior of the walker is not accessible.

Here we develop a general analytical framework to study persistent random walks over the whole range of time scales. The goal is to clarify and disentangle the combined effects of self-propulsion p and the stepping strategy of the walker, consisting of its step-length $\mathcal{F}(\ell)$ and turning-angle $R(\phi)$ distributions. The method enables us to analytically determine the time evolution of arbitrary moments of displacement. Using this approach, the second moment, i.e., the mean-square displacement, has been recently analyzed [4], revealing a variety of signatures of anomalous diffusion on short time scales even in the absence of viscoelasticity, traps, or overcrowding. These elements were frequently identified in the nature of the biological environments and received considerable attention as the possible sources of subdiffusion [9].

An alternative way to interpret the model and its outcome is to consider the motion on complex networks, such as motor proteins on the cytoskeleton. These motors have an effective processivity p (i.e., a tendency to move along the same filament [10–12]) and may switch to a new filament at the intersections of the network. From a coarse-grained perspective, one can describe such motion by a persistent random walk on the

*sadjadi@lusi.uni-sb.de
†shaebani@lusi.uni-sb.de

nodes of the network, thus, $\mathcal{F}(\ell)$ and $R(\phi)$ represent the distributions of the segment length ℓ between neighboring intersections and the angle ϕ between intersecting filaments, respectively. Note that the cytoskeleton is a dynamic network due to the underlying growth and shrinkage of filaments, thus, the structure on which the transport takes place often changes. This justifies the relevance of the proposed stochastic approach, where the network structure is always implicitly given.

Our analytical approach provides a recipe to obtain any arbitrary moment of displacement, yet we extend the calculations to the third and fourth moments, which are of particular interest, e.g., in the evaluation of the skewness and kurtosis, or to obtain the variance $\sigma_{r^2} = \langle r^4\rangle - \langle r^2\rangle^2$ (and thus the standard error) of the mean-square displacement (MSD) of a persistent random walker. σ_{r^2} is also a useful quantity for estimating the first moment $\langle r\rangle$ of the net displacement: In the absence of an exact analytical solution for $\langle r\rangle$, an approximate expression $\langle r\rangle \approx \sqrt{\langle r^2\rangle}(1 - \frac{1}{8}\frac{\sigma_{r^2}}{\langle r^2\rangle^2})$ was proposed [13] by means of a Taylor expansion of the square-root function. The asymptotic behavior is, however, shown to follow $\langle r\rangle = \frac{1}{2}\sqrt{\pi\langle r^2\rangle}$ [14].

We first introduce the general approach to obtain arbitrary moments of displacement. Next, an analytical expression is derived for the special case of the mean-square displacement in two dimensions. This part is the full exposition and expansion of the results presented in Ref. [4]. Then we clarify the similarities and differences between the results in two and three dimensions for persistent walks which are symmetric around the previous direction of motion and briefly discuss the case of asymmetric turning-angle distributions in two dimensions. Finally, the calculations are extended to higher moments and cumulants of displacement, and the probability density of the position of the random walker and its time evolution are investigated. The paper is organized in the following manner: Section II contains the description of the master equation formalism for the persistent motion of random walkers in two dimensions. In Sec. III, we discuss symmetric persistent motions in three dimensions. The analytical predictions for MSD are compared with simulation results in Sec. IV. The calculations are extended to higher moments and cumulants of displacement in Sec. V, and the results are compared with simulations. We investigate the parameter dependence and time evolution of the probability distribution of the net distance from the origin in Sec. VI. Moreover, the coupling between longitudinal and perpendicular transport is briefly discussed, and an analytical expression is obtained for the probability that the direction of motion after n steps makes an angle α with the current direction of motion. Section VII concludes the paper.

II. MODEL

We consider the motion of a self-propelled particle as a persistent random walk consisting of steps of different lengths and orientations. Here a two-dimensional motion is introduced and the extension to three dimensions is discussed in the next section. The stochastic motion is described in continuous space and discrete time as follows: At each time step, the particle takes a step of length l along either its previous direction with probability p or a newly chosen direction with

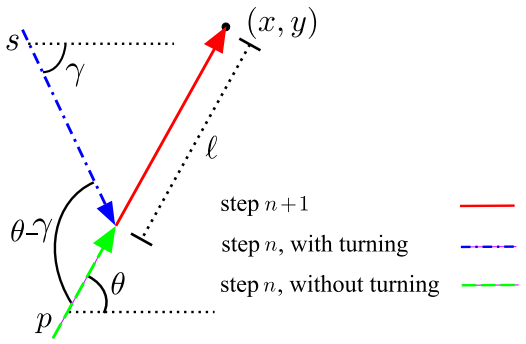

FIG. 1. (Color online) Trajectory of the walker during two successive steps.

probability $s = 1 - p$, as shown in Fig. 1. Thus, p represents the self-propulsion of the particle. We assume probability distributions $R(\phi)$ and $\mathcal{F}(\ell)$ for the rotation angle $\phi = \theta - \gamma$ and the step length l of the walker, respectively. The following master equation expresses the evolution of the probability density $P_n(x,y \mid \theta)$ for the particle to arrive at position (x,y) along the direction θ at time step n:

$$P_{n+1}(x,y \mid \theta) = p \int d\ell\, \mathcal{F}(\ell)\, P_n(x - \ell\cos(\theta), y - \ell\sin(\theta) \mid \theta) + s \int d\ell\, \mathcal{F}(\ell) \int_{-\pi}^{\pi} d\gamma\, R(\theta - \gamma) \times P_n(x - \ell\cos(\theta), y - \ell\sin(\theta) \mid \gamma). \quad (1)$$

The terms on the right-hand side of the above equation correspond to persistent motion with probability p and turning with probability s. One can obtain arbitrary moments of displacement since they are accessible by the derivatives of the Fourier transform of $P_n(x,y \mid \theta)$, which is defined as

$$P_n(\boldsymbol{\omega} \mid m) \equiv \int_{-\pi}^{\pi} d\theta\, e^{im\theta} \int dy \int dx\; e^{i\boldsymbol{\omega}\cdot\mathbf{r}} P_n(x,y \mid \theta). \quad (2)$$

The arbitrary moment $\langle x^{k_1} y^{k_2}\rangle$ is given by

$$\langle x^{k_1} y^{k_2}\rangle_n \equiv \int d\theta \int dy \int dx\; x^{k_1} y^{k_2} P_n(x,y \mid \theta) = (-i)^{k_1+k_2} \frac{\partial^{k_1+k_2} P_n(\omega_x,\omega_y \mid m=0)}{\partial\omega_x^{k_1}\partial\omega_y^{k_2}}\bigg|_{(\omega_x,\omega_y)=(0,0)}. \quad (3)$$

To study the diffusive behavior of particles one deals with the first and second moments of $P_n(x,y \mid \theta)$, namely $\langle x\rangle$, $\langle y\rangle$, $\langle x^2\rangle$, and $\langle y^2\rangle$. Thus, we first focus on the derivation of these quantities in the following. The same procedure is followed in Sec. V to obtain higher moments of displacement. A similar Fourier-Z-transform technique was applied to study diffusive transport of light in foams [15]. The first two moments along the x direction are given by

$$\langle x\rangle_n \equiv -i \frac{\partial P_n(\omega_x,\omega_y \mid m=0)}{\partial\omega_x}\bigg|_{(\omega_x,\omega_y)=(0,0)},$$
$$\langle x^2\rangle_n \equiv (-i)^2 \frac{\partial^2 P_n(\omega_x,\omega_y \mid m=0)}{\partial\omega_x^2}\bigg|_{(\omega_x,\omega_y)=(0,0)}. \quad (4)$$

Similar expressions can be written for $\langle y\rangle$ and $\langle y^2\rangle$. Fourier transforming Eq. (1), we find

$$P_{n+1}(\omega,\alpha\,|\,m) = \sum_{k=-\infty}^{\infty}\Big[i^k e^{-ik\alpha}P_n(\omega,\alpha\,|\,m+k) \times [p+s\,\mathcal{R}(m+k)]\int d\ell\,\mathcal{F}(\ell)J_k(\omega\ell)\Big], \tag{5}$$

where $J_k(z)=\frac{1}{2\pi i^k}\int_{-\pi}^{\pi}d\theta\; e^{iz\cos\theta}e^{-ik\theta}$ is the kth order Bessel's function and $\mathcal{R}(m)=\int_{-\pi}^{\pi}d\phi\; e^{im\phi}R(\phi)$ is the Fourier transform of the rotation angle distribution $R(\phi)$. One can expand $P_n(\omega,\alpha\,|\,m)$ as a Taylor series,

$$P_n(\omega,\alpha\,|\,m) = Q_{0,n}(\alpha\,|\,m) + i\omega\,\langle\ell\rangle\,Q_{1,n}(\alpha\,|\,m) - \tfrac{1}{2}\omega^2\,\langle\ell^2\rangle\,Q_{2,n}(\alpha\,|\,m)+\cdots, \tag{6}$$

with $\langle\ell\rangle$ and $\langle\ell^2\rangle$ being the first and second moments of the step-length distribution $\mathcal{F}(\ell)$. From Eqs. (4) and (6) we obtain the moments in terms of the Taylor expansion coefficients $Q_{i,n}(\alpha\,|\,m)$:

$$\begin{aligned}
\langle x\rangle_n &= \int d\ell\,\mathcal{F}(\ell)\,\ell\;Q_{1,n}(0\,|\,0) = \langle\ell\rangle\,Q_{1,n}(0\,|\,0),\\
\langle y\rangle_n &= \int d\ell\,\mathcal{F}(\ell)\,\ell\;Q_{1,n}\left(\frac{\pi}{2}\,\middle|\,0\right) = \langle\ell\rangle\,Q_{1,n}\left(\frac{\pi}{2}\,\middle|\,0\right),\\
\langle x^2\rangle_n &= \int d\ell\,\mathcal{F}(\ell)\,\ell^2\;Q_{2,n}(0\,|\,0) = \langle\ell^2\rangle\,Q_{2,n}(0\,|\,0),\\
\langle y^2\rangle_n &= \int d\ell\,\mathcal{F}(\ell)\,\ell^2\;Q_{2,n}\left(\frac{\pi}{2}\,\middle|\,0\right) = \langle\ell^2\rangle\,Q_{2,n}\left(\frac{\pi}{2}\,\middle|\,0\right).
\end{aligned} \tag{7}$$

By Taylor expansion of both sides of Eq. (5), one can collect all terms with the same power in ω, leading to the following recursion relations for the Taylor coefficients $Q_{0,n}(\alpha\,|\,m)$, $Q_{1,n}(\alpha\,|\,m)$, and $Q_{2,n}(\alpha\,|\,m)$:

$$Q_{0,n+1}(\alpha\,|\,m) = Q_{0,n}(\alpha\,|\,m)[p+s\,\mathcal{R}(m)], \tag{8}$$

$$\begin{aligned}
Q_{1,n+1}(\alpha\,|\,m) = {}& Q_{1,n}(\alpha\,|\,m)[p+s\,\mathcal{R}(m)]\\
&+\tfrac{1}{2}\{e^{i\alpha}Q_{0,n}(\alpha\,|\,m-1)[p+s\,\mathcal{R}(m-1)]\\
&+e^{-i\alpha}Q_{0,n}(\alpha\,|\,m+1)[p+s\,\mathcal{R}(m+1)]\},
\end{aligned} \tag{9}$$

$$\begin{aligned}
Q_{2,n+1}(\alpha\,|\,m) = {}& \left[\frac{1}{2}Q_{0,n}(\alpha\,|\,m)+Q_{2,n}(\alpha\,|\,m)\right][p+s\,\mathcal{R}(m)]\\
&+\frac{\langle\ell\rangle^2}{\langle\ell^2\rangle}\{e^{i\alpha}Q_{1,n}(\alpha\,|\,m-1)[p+s\,\mathcal{R}(m-1)]\\
&+e^{-i\alpha}Q_{1,n}(\alpha\,|\,m+1)[p+s\,\mathcal{R}(m+1)]\}\\
&+\frac{1}{4}e^{2i\alpha}Q_{0,n}(\alpha\,|\,m-2)[p+s\,\mathcal{R}(m-2)]\\
&+\frac{1}{4}e^{-2i\alpha}Q_{0,n}(\alpha\,|\,m+2)[p+s\,\mathcal{R}(m+2)].
\end{aligned} \tag{10}$$

The coupled linear equations (8), (9), and (10) can be solved by means of the z-transform technique. The z transform $G(z)$ of a function G_n of a discrete variable $n=0,1,2,\ldots$, is defined as

$$G(z)=\sum_{n=0}^{\infty}G_n z^{-n}. \tag{11}$$

By applying the z transform to Eqs. (8)–(10), one obtains a set of algebraic equations for $Q_0(z,\alpha\,|\,m)$, $Q_1(z,\alpha\,|\,m)$, and $Q_2(z,\alpha\,|\,m)$ quantities (see Appendix A).

A. The quantities of interest

The main goal is to evaluate $\langle x\rangle_n$, $\langle y\rangle_n$, $\langle x^2\rangle_n$, and $\langle y^2\rangle_n$, which are given in terms of $Q_{i,n}(\alpha\,|\,m)$ quantities in Eq. (7). Here we derive $\langle x\rangle_n$ and $\langle x^2\rangle_n$, and a similar approach can be followed to obtain $\langle y\rangle_n$ and $\langle y^2\rangle_n$. The z transform of Eq. (7) leads to the following expressions in z space:

$$\begin{aligned}
\langle x\rangle(z) &= \sum_{n=0}^{\infty}z^{-n}\langle\ell\rangle\,Q_{1,n}(0\,|\,0) = \langle\ell\rangle\,Q_1(z,0\,|\,0),\\
\langle x^2\rangle(z) &= \sum_{n=0}^{\infty}z^{-n}\langle\ell^2\rangle\,Q_{2,n}(0\,|\,0) = \langle\ell^2\rangle\,Q_2(z,0\,|\,0).
\end{aligned} \tag{12}$$

From Eqs. (12), (A2), and (A3), one obtains the first and second moments of x in the z space [see Eqs. (B1) and (B2) in Appendix B]. The last step to get the moments $\langle x\rangle$ and $\langle x^2\rangle$ in real time is the inverse z transforming of the z-space moments [i.e., Eqs. (B1) and (B2)]. By introducing $A_i=p+s\,\mathcal{R}(i)$, the resulting moments are

$$\langle x\rangle_n = \langle\ell\rangle\,Q_{1,n=0}(0\,|\,0)+\frac{\langle\ell\rangle}{2}Q_{0,n=0}(0\,|\,-1)A_{-1}\frac{1-A_{-1}^n}{1-A_{-1}}+\frac{\langle\ell\rangle}{2}Q_{0,n=0}(0\,|\,1)A_1\frac{1-A_1^n}{1-A_1}, \tag{13}$$

$$\begin{aligned}
\langle x^2\rangle_n = {}& \langle\ell^2\rangle Q_{2,n=0}(0\,|\,0)+n\frac{\langle\ell^2\rangle}{2}Q_{0,n=0}(0\,|\,0)+\langle\ell\rangle^2 Q_{1,n=0}(0\,|\,-1)A_{-1}\frac{1-A_{-1}^n}{1-A_{-1}}+\langle\ell\rangle^2 Q_{1,n=0}(0\,|\,1)A_1\frac{1-A_1^n}{1-A_1}\\
&+\frac{\langle\ell\rangle^2}{2}Q_{0,n=0}(0\,|\,-2)\,A_{-1}\,A_{-2}\times\frac{A_{-1}^nA_{-2}+A_{-2}^n(A_{-1}-1)+A_{-2}-A_{-1}}{(A_{-1}-A_{-2})\,(A_{-2}-1)\,(1-A_{-1})}+\frac{\langle\ell\rangle^2}{2}Q_{0,n=0}(0\,|\,2)\,A_1\,A_2\\
&\times\frac{A_1^nA_2+A_2^n(A_1-1)+A_2-A_1}{(A_1-A_2)\,(A_2-1)\,(1-A_1)}+\frac{\langle\ell\rangle^2}{2}Q_{0,n=0}(0\,|\,0)\left[A_{-1}\frac{A_{-1}^n-A_{-1}n+n-1}{(1-A_{-1})^2}+A_1\frac{A_1^n-A_1n+n-1}{(1-A_1)^2}\right]\\
&+\frac{\langle\ell^2\rangle}{4}Q_{0,n=0}(0\,|\,-2)A_{-2}\frac{1-A_{-2}^n}{1-A_{-2}}+\frac{\langle\ell^2\rangle}{4}Q_{0,n=0}(0\,|\,2)A_2\frac{1-A_2^n}{1-A_2}.
\end{aligned} \tag{14}$$

B. Isotropic initial condition

For the isotropic initial condition $P_0(x,y \mid \theta) = \frac{1}{2\pi}\delta(x)\delta(y)$, one finds from Eq. (2) that $P_0(\boldsymbol{\omega}|m)=\frac{1}{2\pi}\int_{-\pi}^{\pi} d\theta\, e^{im\theta}=\frac{\sin(m\pi)}{m\pi}$. Then, using the expansion equation (6) for $\omega = 0$, it can be seen that the only nonzero Q quantity is $Q_{0,n=0}(\alpha \mid 0) = 1$ (for $m = 0$). Therefore, Eq. (14) leads to

$$\langle x\rangle_n = 0, \tag{15}$$

and Eq. (14), after replacing s with $1 - p$, reads

$$\langle x^2\rangle_n = n\frac{\langle\ell\rangle^2}{2}\left\{\lambda + \frac{[p+\mathcal{R}(1)-p\mathcal{R}(1)]}{(1-p)[1-\mathcal{R}(1)]} + \frac{[p+\mathcal{R}(-1)-p\mathcal{R}(-1)]}{(1-p)[1-\mathcal{R}(-1)]}\right\} + \frac{\langle\ell\rangle^2}{2}\frac{[p+\mathcal{R}(1)-p\mathcal{R}(1)]}{(1-p)^2[1-\mathcal{R}(1)]^2}\{[p+\mathcal{R}(1)-p\mathcal{R}(1)]^n - 1\}$$
$$+ \frac{\langle\ell\rangle^2}{2}\frac{[p+\mathcal{R}(-1)-p\mathcal{R}(-1)]}{(1-p)^2[1-\mathcal{R}(-1)]^2}\{[p+\mathcal{R}(-1)-p\mathcal{R}(-1)]^n - 1\}, \tag{16}$$

with $\lambda = \langle\ell^2\rangle/\langle\ell\rangle^2$ being the relative variance of the step-length distribution. The y component of the mean-square displacement $\langle y^2\rangle_n$ has the same form as shown in Eq. (16) due to symmetry. Therefore, one obtains $\langle r^2\rangle_n = \langle x^2\rangle_n + \langle y^2\rangle_n = 2\langle x^2\rangle_n$.

C. Long-time behavior

From Eq. (16) in the limit of long time (i.e., $n\to\infty$) one obtains the asymptotic mean-square displacement as

$$\langle r^2\rangle_n/\langle\ell\rangle^2 \simeq n\left\{\lambda + \frac{[p+\mathcal{R}(1)-p\mathcal{R}(1)]}{(1-p)[1-\mathcal{R}(1)]} + \frac{[p+\mathcal{R}(-1)-p\mathcal{R}(-1)]}{(1-p)[1-\mathcal{R}(-1)]}\right\} - \frac{[p+\mathcal{R}(1)-p\mathcal{R}(1)]}{(1-p)^2[1-\mathcal{R}(1)]^2} - \frac{[p+\mathcal{R}(-1)-p\mathcal{R}(-1)]}{(1-p)^2[1-\mathcal{R}(-1)]^2}. \tag{17}$$

Assuming that the particle moves with a constant speed v during the ballistic parts of motion, the elapsed time after n steps is $\tau = n\langle\ell\rangle/v$. The diffusion constant D is related to $\langle r^2\rangle_n$ as

$$\langle r^2\rangle_n = 4D\tau, \tag{18}$$

thus, we find

$$D = \frac{v\langle\ell\rangle}{4}\left\{\lambda + \frac{[p+\mathcal{R}(1)-p\mathcal{R}(1)]}{(1-p)[1-\mathcal{R}(1)]} + \frac{[p+\mathcal{R}(-1)-p\mathcal{R}(-1)]}{(1-p)[1-\mathcal{R}(-1)]}\right\}. \tag{19}$$

D. Turning with left-right symmetry

The distribution $R(\phi)$ reflects to what extent the directions of the successive steps are correlated. The analytical method presented in this section allows us to handle an arbitrary function $R(\phi)$; however, we are particularly interested in the distributions with equal probabilities to turn clockwise or anticlockwise. This implies that $\mathcal{R}(1) = \mathcal{R}(-1)(\equiv\mathcal{R})$. The asymmetry of the turning angle with respect to the arrival direction is quantitatively reflected in the value of $\mathcal{R}$ which ranges between -1 and 1, with zero denoting a uniform case and negative (positive) values corresponding to a higher chance of motion to the near backward (forward) directions in the next step. When left-right symmetry holds the imaginary part of $\mathcal{R}(m)$ vanishes, thus, $\mathcal{R}$ becomes

$$\mathcal{R} = \int_{-\pi}^{\pi} d\phi\ \cos(\phi)\ R(\phi), \tag{20}$$

and Eq. (16) reduces to

$$\langle x^2\rangle_n = \frac{1}{2}n\langle\ell\rangle^2\left[\lambda + \frac{2(p+\mathcal{R}-p\mathcal{R})}{(1-p)(1-\mathcal{R})}\right]$$
$$+ \langle\ell\rangle^2\frac{(p+\mathcal{R}-p\mathcal{R})}{(1-p)^2(1-\mathcal{R})^2}[(p+\mathcal{R}-p\mathcal{R})^n - 1]. \tag{21}$$

III. EXTENSION TO THREE DIMENSIONS

The analytical approach of Sec. II can be straightforwardly generalized to the persistent motion in three dimensions by introducing the probability density $P_n(x,y,z \mid \phi,\varphi)$ for the particle to arrive at position (x,y,z) at time step n along the direction characterized by the azimuthal and polar angles ϕ and φ, even though the calculations for the general motion in three dimensions are quite lengthy. However, the processes with symmetric turning-angle distribution are of particular importance since usually the rotational symmetry holds in biological applications. Thus, we restrict ourselves in this section to the turning-angle distributions with cylindrical symmetry with respect to the incoming direction. This is the three-dimensional analog to those processes in two dimensions which obey left-right symmetry.

Similarly to the 2D case, we introduce $R(\phi)$ as the probability of turning with angle ϕ with respect to the incoming direction (see Fig. 2). The polar angle φ is supposed to be uniformly distributed over the range $[0,2\pi]$. Note that, in contrast to the 2D case, the normalization condition of $R(\phi)$ in 3D requires an integration over all possibilities of φ, i.e., $\int_0^{\pi} R(\phi)\,\sin(\phi)\,d\phi = 1$. Here, again, the corresponding Fourier transform of $R(\phi)$ is real. Since every two successive steps lie in a plane, as shown in Fig. 2, one can intuitively write the same two-dimensional master equation [Eq. (1)] to

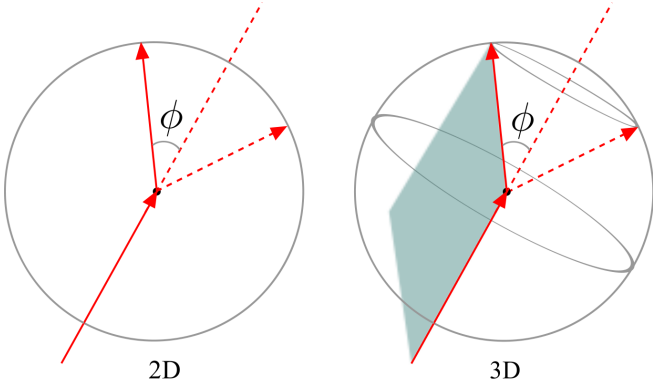

FIG. 2. (Color online) Illustration of symmetric rotations with respect to the incoming direction, in two (left) and three (right) dimensions.

describe the motion in three dimensions. By solving this master equation, one gets a similar expression for $\langle x^2\rangle$ as for the 2D solution presented in Eq. (16) in the case of $\mathcal{R}(1)=\mathcal{R}(-1)$, even though with different prefactors:

$$\langle x^2\rangle_n = n\frac{\langle\ell\rangle^2}{3}\left[\lambda+\frac{2(p+\mathcal{E}-p\,\mathcal{E})}{(1-p)(1-\mathcal{E})}\right] + \frac{2\langle\ell\rangle^2}{3}\frac{(p+\mathcal{E}-p\,\mathcal{E})}{(1-p)^2(1-\mathcal{E})^2}[(p+\mathcal{E}-p\,\mathcal{E})^n-1]. \quad (22)$$

Here $\mathcal{E}$ is the real part of the Fourier transform of the rotation-angle distribution

$$\mathcal{E}=\int_0^\pi d\phi\ \cos(\phi)\ R(\phi)\ \sin(\phi). \quad (23)$$

Finally, one can obtain the total mean-square displacement $\langle r^2\rangle_n=\langle x^2\rangle_n+\langle y^2\rangle_n+\langle z^2\rangle_n$, which has the same form as in 2D, only $\mathcal{R}$ is replaced with $\mathcal{E}$:

$$\langle r^2\rangle_n = n\langle\ell\rangle^2\left[\lambda+\frac{2(p+\mathcal{E}-p\mathcal{E})}{(1-p)(1-\mathcal{E})}\right] + \langle\ell\rangle^2\frac{2(p+\mathcal{E}-p\mathcal{E})}{(1-p)^2(1-\mathcal{E})^2}[(p+\mathcal{E}-p\mathcal{E})^n-1]. \quad (24)$$

IV. SIMULATION RESULTS FOR MSD

In this section we compare the analytical predictions with the results of extensive Monte Carlo simulations obtained from the same step length $\mathcal{F}(\ell)$ and turning-angle $R(\phi)$ distributions and self-propulsion p. The formalism introduced in Secs. II and III enables us to handle any arbitrary function for $R(\phi)$ and $\mathcal{F}(\ell)$; nevertheless, we restrict $R(\phi)$ in this section to symmetric distributions along the incoming direction for simplicity and because of its practical applications in biological systems.

We first investigate the overall behavior of the mean-square displacement for different values of λ, p, and $\mathcal{R}$. λ is a measure of the heterogeneity of the network structure or the diversity of the step sizes, and $\mathcal{R}$ quantifies the anisotropy of the structure or the asymmetry of the turning angles of the walker. The characteristics of the $\mathcal{F}(\ell)$ and $R(\phi)$ distributions can be considered as the stepping strategy of the random walker which may be tunable externally (e.g., by controlling the external agitation imposed on a driven granular system [16]) or internally (by controlling the strength, density, and spatial arrangement of obstacles in the system or by adjusting the underlying structure of the environment such as a porous medium [17]). p is the self-propulsion of the particle (equivalently, the processivity or persistency of the walker). The case $p=\mathcal{R}=0$ and $\lambda=1$ corresponds to a simple diffusion (see Fig. 3). When p and $\mathcal{R}$ are both positive, they cooperate to send the walker to the near forward directions more frequently, resulting in superdiffusion at short time scales. If $\mathcal{R}$ is negative, it competes against p, which may lead to sub-, normal, or superdiffusion. At the extreme negative value of $\mathcal{R}$ (i.e., $\mathcal{R}\to-1$), an oscillatory phase can be observed where the particle experiences a nearly back-and-forth motion [4].

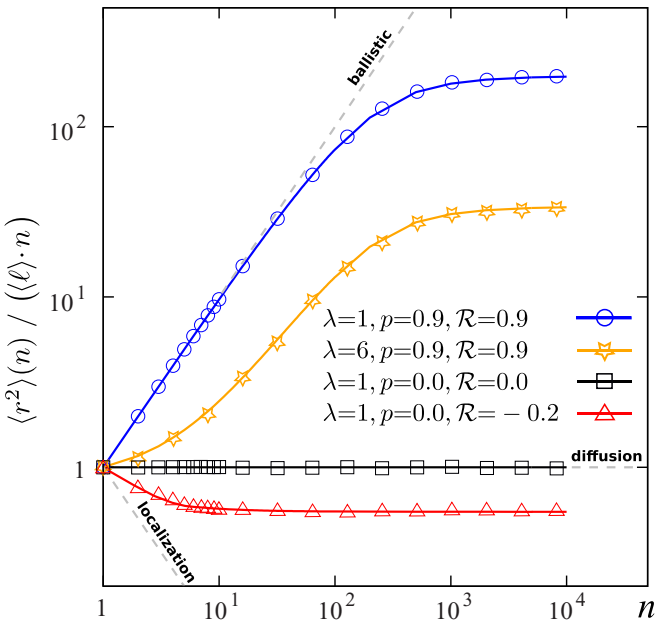

FIG. 3. (Color online) Time evolution of the mean-square displacement $\langle r^2\rangle$ scaled by n for different values of λ, p, and $\mathcal{R}$. The solid lines correspond to analytical predictions via Eq. (21), and the symbols denote simulation results.

It can be seen from Fig. 3 that the asymptotic behavior of all curves is diffusive. This is due to the fact that there is no preferred direction in the system and the effective correlations which exist between successive step angles are short range. The crossover time n_c to asymptotic diffusion can be estimated by balancing the linear and exponential terms in Eq. (21). In Fig. 4(a), n_c is shown as a function of self-propulsion for several values of $\mathcal{R}$ and λ. Increasing p and/or $\mathcal{R}$ delays the crossover, while the walker gets randomized more quickly for strong heterogeneities. The asymptotic diffusion coefficient varies by several orders of magnitude with control parameters p, $\mathcal{R}$, and λ [see Fig. 4(b)].

A remarkable outcome of the analytical formalism is that the anomalous diffusive motion of the particle is fully described by the self-propulsion and the characteristics of the step-length and turning-angle distributions, namely the first two moments $\langle\ell\rangle$ and $\langle\ell^2\rangle$ of $\mathcal{F}(\ell)$ and the Fourier transform of $R(\phi)$. Therefore, one expects that stepping with different distributions but with the same key characteristics

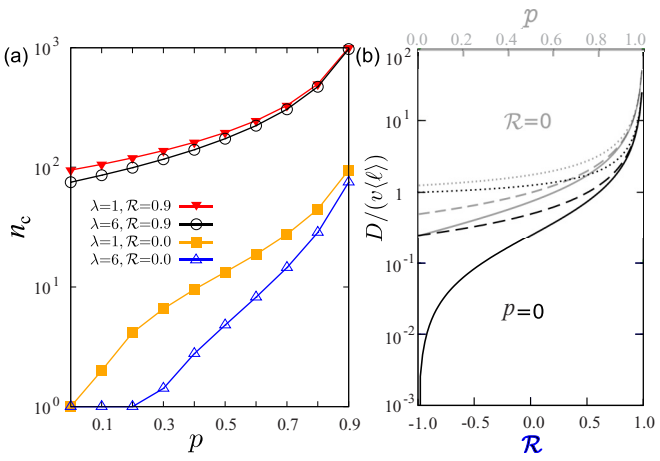

FIG. 4. (Color online) (a) The crossover time n_c to the asymptotic diffusive regime versus self-propulsion p. (b) The asymptotic diffusion coefficient D in terms of self-propulsion p (light gray curves) or anisotropy $\mathcal{R}$ (dark gray curves). The solid, dashed, and dotted lines correspond to $\lambda = 1,2,5$, respectively.

mentioned above should lead to the same results, independent of the functional form of the distributions. To verify this finding by simulations, we first choose an isotropic distribution $R(\phi) = \frac{1}{2\pi}$ and compare two different step-length distributions with the same $\langle\ell\rangle$ and $\langle\ell^2\rangle$ moments. As shown in Fig. 5, the simulation results match remarkably for an exponential function $\mathcal{F}(\ell) = e^{1-\ell}$ and a uniform distribution $\mathcal{F}(\ell) = \frac{H(\ell-\ell_{\min})+H(\ell_{\max}-\ell)-1}{\ell_{\max}-\ell_{\min}}$ [$H(x)$ is the Heaviside step function], both with $\langle\ell\rangle = 2$ and $\langle\ell^2\rangle = 5$.

Next, we choose a given step-length distribution [either $\mathcal{F}(\ell) = \delta(\ell-1)$ or $\mathcal{F}(\ell) = e^{1-\ell}$] and compare three different turning-angle distributions: a uniform function $R_1(\phi) = \frac{1}{2\pi}$, a motion restricted to left or right directions $R_2(\phi) = \frac{1}{2}[\delta(\phi+\pi/2)+\delta(\phi-\pi/2)]$, and a motion restricted to forward or backward directions $R_3(\phi) = \frac{1}{2}[\delta(\phi)+\delta(\phi-\pi)]$.

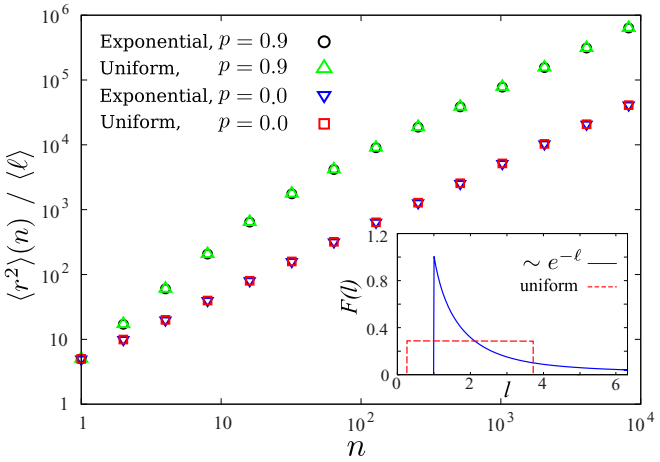

FIG. 5. (Color online) Time evolution of $\langle r^2\rangle$ for two different distributions $\mathcal{F}(\ell)$ with the same moments $\langle\ell\rangle = 2$ and $\langle\ell^2\rangle = 5$ ($\lambda = 1.25$). Inset: Comparison between the exponential distribution $\mathcal{F}(\ell) = e^{1-\ell}$ ($\ell \in [1,\infty]$) and the uniform distribution $\mathcal{F}(\ell) = \frac{H(\ell-\ell_{\min})+H(\ell_{\max}-\ell)-1}{\ell_{\max}-\ell_{\min}}$ ($\ell_{\min} = 0.268$, $\ell_{\max} = 3.732$).

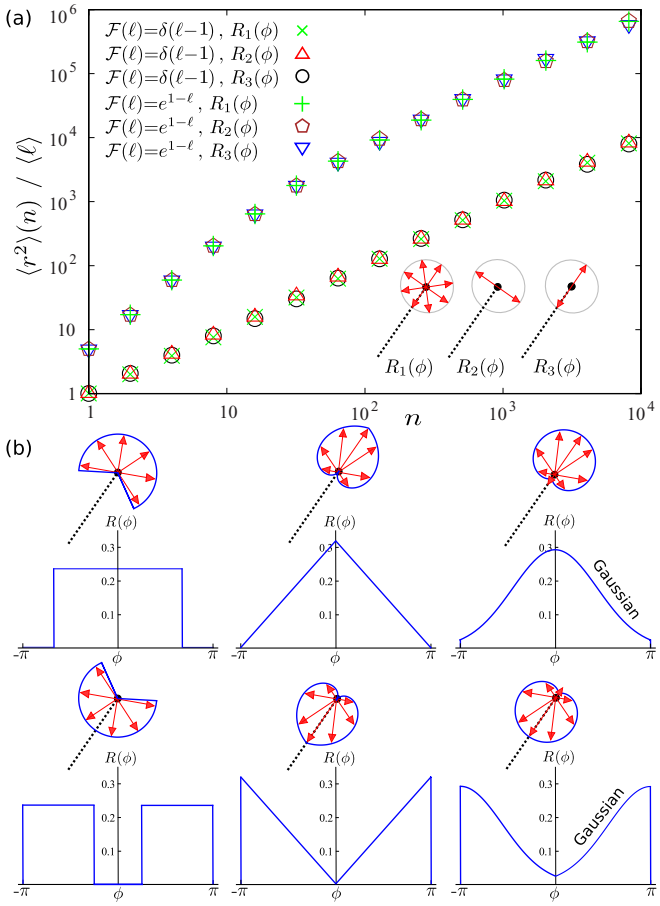

FIG. 6. (Color online) (a) Mean-square displacement $\langle r^2\rangle$ vs n for three different distributions $R(\phi)$ with $\mathcal{R} = 0$ given in the text. The step-length distribution is chosen to be either $\mathcal{F}(\ell) = \delta(\ell-1)$ (with $p = 0$) or $\mathcal{F}(\ell) = e^{1-\ell}$ (with $p = 0.9$). Insets: The possible directions of motion at the next step for each $R(\phi)$. (b) A few sample distributions $R(\phi)$ with $\mathcal{R} \simeq 0.4$ (top) and $\mathcal{R} \simeq -0.4$ (bottom). The dotted lines show the arrival direction and the arrows indicate the possible directions in the next step, with length being proportional to the probability.

All these examples correspond to $\mathcal{R} = 0$, i.e., on average, they have no preference for forward or backward motion. Figure 6(a) reveals that there is a perfect agreement between the simulation results obtained for these different turning-angle distributions. One can also generate positive or negative values of $\mathcal{R}$ from different $R(\phi)$ distributions. Several examples are shown in Fig. 6(b) for $\mathcal{R} \simeq 0.4$ (or $\mathcal{R} \simeq -0.4$), which all lead to the same diffusive motion.

So far, only symmetric distributions have been studied. Now we briefly investigate turning-angle distributions which are asymmetric with respect to the incoming direction. Let us consider two-dimensional walks for simplicity. An asymmetric $R(\phi)$ in this case means that the left-right symmetry of turning is broken, leading to (anti-)clockwise spiral trajectories. A comparison is made in Fig. 7 between the trajectories obtained from three different uniform distributions over the range $(\phi_{\min},\phi_{\max})$: $R_1(\phi)$ is an isotropic function corresponding to a normal diffusion [$\mathcal{R} \equiv \mathcal{R}(+1) = \mathcal{R}(-1) = 0$], $R_2(\phi)$ is a symmetric function ($\phi_{\min} = -\pi/6$, $\phi_{\max} = \pi/6$) which results in $\mathcal{R} \equiv \mathcal{R}(+1) = \mathcal{R}(-1) \simeq 0.95$, and $R_3(\phi)$

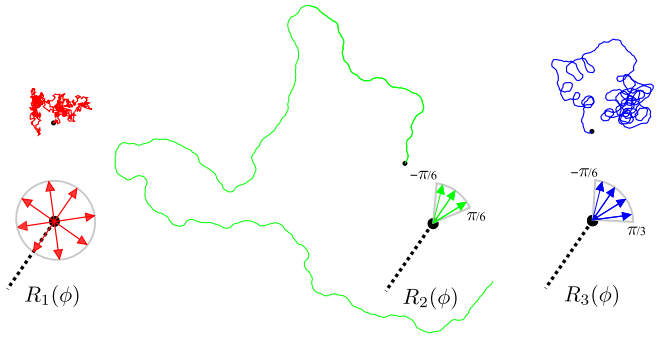

FIG. 7. (Color online) Typical trajectories at $p = 0$ and $\lambda = 1$ for isotropic (left), forward symmetric (middle), and forward asymmetric (right) turning-angle distributions, after the same number of steps. The arrows show possible directions of motion in the next step.

is an asymmetric distribution over the range $[-\pi/6,\pi/3]$ which creates clockwise spirals. Here $\mathcal{R}(+1) \simeq 0.87 + i\,0.23$ and $\mathcal{R}(-1) \simeq 0.87 - i\,0.23$, thus, $\mathcal{R}(+1) \neq \mathcal{R}(-1)$. The asymptotic diffusion coefficient [Eq. (19)] is, however, a real number $D/v\langle\ell\rangle = \frac{1}{4}[\lambda + 2\frac{A-A^2-B^2}{(1-A)^2+B^2}]$ in the absence of self-propulsion, with A and B being the real and imaginary parts of $\mathcal{R}(\pm 1)$. We obtain $D/(v\langle\ell\rangle/4) \simeq 1.0$, 43.4, and 2.7 for $R_1(\phi)$, $R_2(\phi)$, and $R_3(\phi)$, respectively, in agreement with the simulation results.

V. HIGHER MOMENTS AND CUMULANTS

The procedure described in Sec. II enables one to obtain any arbitrary moment of displacement. To better clarify the proposed recipe, we extend the calculations to the third and fourth moments in this section, which are sufficient to derive up to the fourth cumulants of displacement and obtain the skewness and kurtosis of a persistent random walk which are measures for the asymmetry and peakedness of the probability distribution, respectively. We also compare the analytical predictions with Monte Carlo simulation results.

From Eq. (3), the third and fourth moments of the displacement are given by

$$\langle x^3\rangle_n \equiv (-i)^3 \frac{\partial^3 P_n(\omega_x,\omega_y \mid m=0)}{\partial\omega_x^3}\bigg|_{(\omega_x,\omega_y)=(0,0)} \tag{25}$$

and

$$\langle x^4\rangle_n \equiv (-i)^4 \frac{\partial^4 P_n(\omega_x,\omega_y \mid m=0)}{\partial\omega_x^4}\bigg|_{(\omega_x,\omega_y)=(0,0)}. \tag{26}$$

Moreover, by expanding $P_n(\omega,\alpha \mid m)$ up to the fourth-order terms in ω one finds

$$\begin{aligned} P_n(\omega,\alpha \mid m) = {} & Q_{0,n}(\alpha \mid m) + i\omega\,\langle\ell\rangle\, Q_{1,n}(\alpha \mid m) \\ & - \frac{1}{2}\omega^2\,\langle\ell^2\rangle\, Q_{2,n}(\alpha \mid m) - \frac{i}{6}\omega^3\,\langle\ell^3\rangle\, Q_{3,n}(\alpha \mid m) \\ & + \frac{1}{24}\omega^4\,\langle\ell^4\rangle\, Q_{4,n}(\alpha \mid m) + \cdots, \end{aligned} \tag{27}$$

which results in the following relations between $\langle x^3\rangle$ or $\langle x^4\rangle$ and the Taylor expansion coefficients:

$$\begin{aligned} \langle x^3\rangle_n &= \int d\ell\,\mathcal{F}(\ell)\ell^3 Q_{3,n}(0 \mid 0) = \langle\ell^3\rangle Q_{3,n}(0 \mid 0), \\ \langle x^4\rangle_n &= \int d\ell\,\mathcal{F}(\ell)\ell^4 Q_{4,n}(0 \mid 0) = \langle\ell^4\rangle Q_{4,n}(0 \mid 0). \end{aligned} \tag{28}$$

Then, by following the procedure introduced in Sec. II, one obtains recursion relations for $Q_{3,n}(\alpha \mid m)$ and $Q_{4,n}(\alpha \mid m)$ as

$$\begin{aligned} Q_{3,n+1}(\alpha \mid m) = {} & \left[\frac{3}{2}\frac{\langle\ell\rangle\langle\ell^2\rangle}{\langle\ell^3\rangle} Q_{1,n}(\alpha \mid m) + Q_{3,n}(\alpha \mid m)\right][p + s\,\mathcal{R}(m)] + \left[\frac{\langle\ell\rangle\langle\ell^2\rangle}{\langle\ell^3\rangle} Q_{2,n}(\alpha \mid m+1) + \frac{1}{4}Q_{0,n}(\alpha \mid m+1)\right] \\ & \times \frac{3}{2}e^{-i\alpha}[p + s\,\mathcal{R}(m+1)] + \left[\frac{\langle\ell\rangle\langle\ell^2\rangle}{\langle\ell^3\rangle} Q_{2,n}(\alpha \mid m-1) + \frac{1}{4}Q_{0,n}(\alpha \mid m-1)\right] \times \frac{3}{2}e^{i\alpha}[p + s\,\mathcal{R}(m-1)] \\ & + \left[\frac{\langle\ell\rangle\langle\ell^2\rangle}{\langle\ell^3\rangle} Q_{1,n}(\alpha \mid m+2)\right]\frac{3}{4}e^{-2i\alpha}[p + s\,\mathcal{R}(m+2)] + \left[\frac{\langle\ell\rangle\langle\ell^2\rangle}{\langle\ell^3\rangle} Q_{1,n}(\alpha \mid m-2)\right]\frac{3}{4}e^{2i\alpha}[p + s\,\mathcal{R}(m-2)] \\ & + \frac{1}{8}e^{-3i\alpha}Q_{0,n}(\alpha \mid m+3)[p + s\,\mathcal{R}(m+3)] + \frac{1}{8}e^{3i\alpha}Q_{0,n}(\alpha \mid m-3)[p + s\,\mathcal{R}(m-3)] \end{aligned} \tag{29}$$

and

$$\begin{aligned} Q_{4,n+1}(\alpha \mid m) = {} & \left[\frac{3}{8}Q_{0,n}(\alpha \mid m) + 3\frac{\langle\ell^2\rangle^2}{\langle\ell^4\rangle} Q_{2,n}(\alpha \mid m) + Q_{4,n}(\alpha \mid m)\right][p + s\,\mathcal{R}(m)] \\ & + e^{-i\alpha}\left[2\frac{\langle\ell\rangle\langle\ell^3\rangle}{\langle\ell^4\rangle} Q_{3,n}(\alpha \mid m+1) + \frac{3}{2}\frac{\langle\ell\rangle\langle\ell^3\rangle}{\langle\ell^4\rangle} Q_{1,n}(\alpha \mid m+1)\right][p + s\,\mathcal{R}(m+1)] \\ & + e^{i\alpha}\left[2\frac{\langle\ell\rangle\langle\ell^3\rangle}{\langle\ell^4\rangle} Q_{3,n}(\alpha \mid m-1) + \frac{3}{2}\frac{\langle\ell\rangle\langle\ell^3\rangle}{\langle\ell^4\rangle} Q_{1,n}(\alpha \mid m-1)\right][p + s\,\mathcal{R}(m-1)] \\ & + e^{-2i\alpha}\left[\frac{3}{2}\frac{\langle\ell^2\rangle^2}{\langle\ell^4\rangle} Q_{2,n}(\alpha \mid m+2) + \frac{1}{4}Q_{0,n}(\alpha \mid m+2)\right][p + s\,\mathcal{R}(m+2)] \end{aligned}$$

$$+e^{2i\alpha}\left[\frac{3}{2}\frac{\langle\ell^2\rangle^2}{\langle\ell^4\rangle}Q_{2,n}(\alpha\mid m-2)+\frac{1}{4}Q_{0,n}(\alpha\mid m-2)\right][p+s\,\mathcal{R}(m-2)]$$
$$+\frac{1}{2}e^{-3i\alpha}\frac{\langle\ell\rangle\langle\ell^3\rangle}{\langle\ell^4\rangle}Q_{1,n}(\alpha\mid m+3)[p+s\,\mathcal{R}(m+3)]+\frac{1}{2}e^{3i\alpha}\frac{\langle\ell\rangle\langle\ell^3\rangle}{\langle\ell^4\rangle}Q_{1,n}(\alpha\mid m-3)[p+s\,\mathcal{R}(m-3)]$$
$$+\frac{1}{16}e^{-4i\alpha}Q_{0,n}(\alpha\mid m+4)[p+s\,\mathcal{R}(m+4)]+\frac{1}{16}e^{4i\alpha}Q_{0,n}(\alpha\mid m-4)[p+s\,\mathcal{R}(m-4)]. \quad (30)$$

The corresponding algebraic equations for $Q_3(z,\alpha\mid m)$ and $Q_4(z,\alpha\mid m)$ after the z transform are given in Appendix A. From Eq. (28), the third and fourth moments of x in the z space can be obtained as

$$\langle x^3\rangle(z)=\sum_{n=0}^{\infty}z^{-n}\langle\ell^3\rangle\,Q_{3,n}(0\mid 0)=\langle\ell^3\rangle\,Q_3(z,0\mid 0),$$
$$\langle x^4\rangle(z)=\sum_{n=0}^{\infty}z^{-n}\langle\ell^4\rangle\,Q_{4,n}(0\mid 0)=\langle\ell^4\rangle\,Q_4(z,0\mid 0). \quad (31)$$

By inserting $Q_3(z,0\mid 0)$ and $Q_4(z,0\mid 0)$ from Eqs. (A4) and (A5), and inverse z transforming of the z-space moments, we finally obtain $\langle x^3\rangle_n$ and $\langle x^4\rangle_n$, which are very lengthy equations. However, they fortunately reduce to simpler forms when we consider the most interesting cases. For example, the isotropic initial condition leads to

$$\langle x^3\rangle_n=0, \quad (32)$$

and if we further limit the motion to a constant step size, $\mathcal{F}(\ell)=\delta(\ell-L)$, and turning with left-right symmetry, the resulting $\langle x^4\rangle_n$ reads

$$\langle x^4\rangle_n=\frac{-3}{8}L^4\Bigg(-\frac{2(A_1+A_2)^2A_2^{n+1}}{(1-A_2)^2(A_1-A_2)^2}+\frac{4A_1^{n+1}(n+1)[A_1(3A_1+1)-A_2(A_1+3)]}{(1-A_1)^3(A_1-A_2)}$$
$$+\frac{4A_1^{n+1}\{-8(2+A_1)A_1^2A_2+[A_1(7A_1+4)+1]A_1^2+[A_1(3A_1+8)+1]A_2^2\}}{(1-A_1)^4(A_1-A_2)^2}$$
$$+\frac{(n+1)(1+A_1)[-3A_1^2+(A_1-3)(5A_1+3)A_2+12A_1+7]}{(1-A_1)^3(1-A_2)}-\frac{2(n+1)(n+2)(1+A_1)^2}{(1-A_1)^2}$$
$$+\frac{2A_1A_2(A_1^3+18A_1+24)-A_2^2(A_1+1)\{A_1[(A_1-5)A_1+23]+5\}+A_1(A_1+2)[(A_1-6)A_1-10]+10A_2-3}{(1-A_1)^4(1-A_2)^2}\Bigg), \quad (33)$$

with

$$A_1=p+s\,\mathcal{R}(1)=p+s\int_{-\pi}^{\pi}d\phi\,\cos(\phi)\,R(\phi),$$
$$A_2=p+s\,\mathcal{R}(2)=p+s\int_{-\pi}^{\pi}d\phi\,\cos(2\phi)\,R(\phi).$$

The analytical prediction for $\langle x^4\rangle_n$ via Eq. (33) is in agreement with the simulation results as shown in Fig. 8. It can be seen that $\langle x^4\rangle_n$ contains similar information as the MSD concerning the anomalous diffusive motion of the persistent walker.

The cumulants are often used in the statistical analysis as an alternative to the moments of the distribution. In general, the following relations hold between the n-th cumulant κ_n and the moments (shown up to the 4th cumulant):

$$\kappa_1=\langle x\rangle,$$
$$\kappa_2=\langle x^2\rangle-\langle x\rangle^2,$$
$$\kappa_3=\langle x^3\rangle-3\langle x^2\rangle\langle x\rangle+2\langle x\rangle^3,$$
$$\kappa_4=\langle x^4\rangle-4\langle x^3\rangle\langle x\rangle-3\langle x^2\rangle^2+12\langle x^2\rangle\langle x\rangle^2-6\langle x\rangle^4. \quad (34)$$

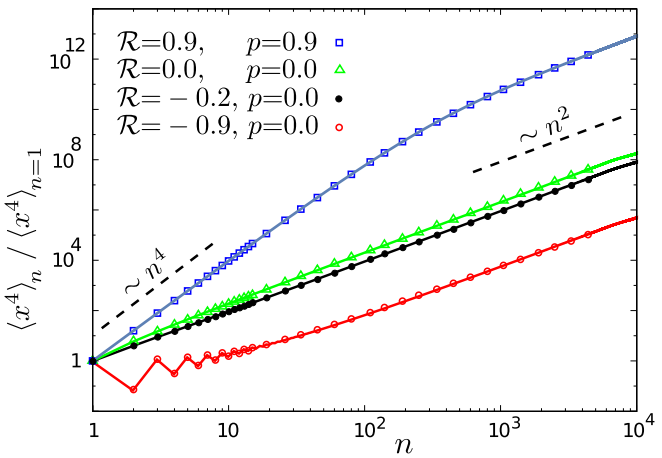

FIG. 8. (Color online) Time evolution of the fourth moment of displacement for different values of λ, p, and $\mathcal{R}$. The solid lines correspond to analytical predictions and the symbols denote simulation results.

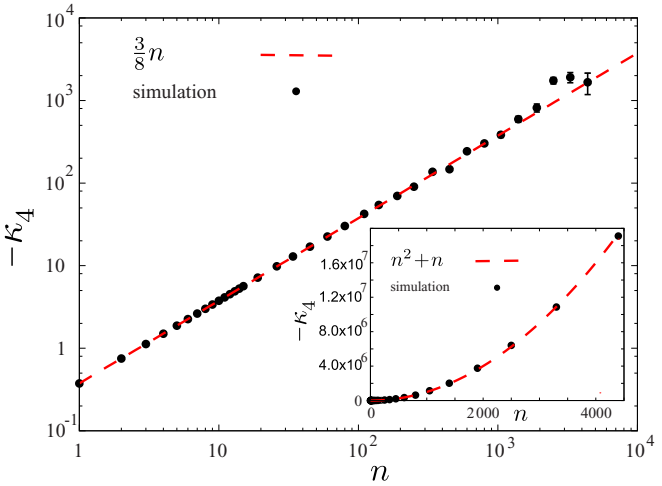

FIG. 9. (Color online) The fourth cumulant of x (in units of $\langle \ell^4 \rangle$) in terms of n for a random walk with $p = A_1 = A_2 = 0$. Inset: The corresponding fourth cumulant of the net displacement r vs n.

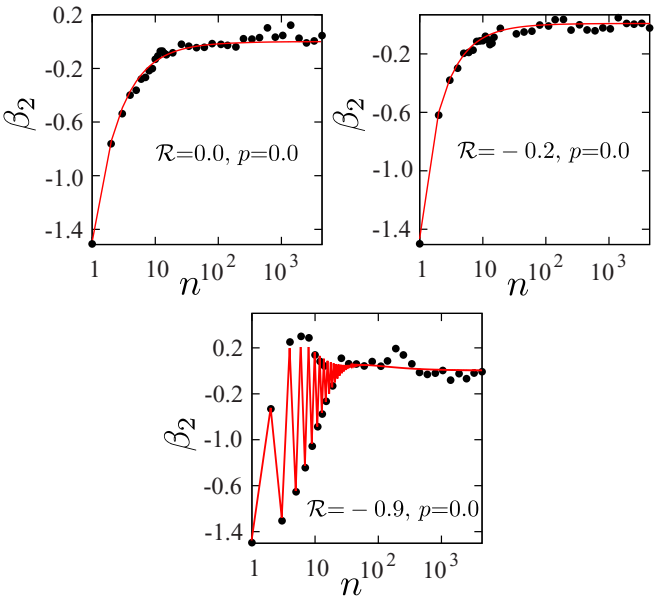

FIG. 10. (Color online) The kurtosis measure β_2 in terms of the step number n for different turning-angle distributions. The lines correspond to analytical predictions via Eq. (36) and the symbols denote simulation results.

If the walker starts from the origin with the isotropic initial condition, the odd moments equal zero and the cumulant-moment relations reduce to

$$\begin{aligned} \kappa_1 &= 0, \\ \kappa_2 &= \langle x^2 \rangle, \\ \kappa_3 &= 0, \\ \kappa_4 &= \langle x^4 \rangle - 3\langle x^2 \rangle^2. \end{aligned} \tag{35}$$

In the case of an ordinary random walk with $\mathcal{F}(\ell) = \delta(\ell - L)$, we have $p = A_1 = A_2 = 0$, $\langle x^2 \rangle / L^2 = \frac{1}{2}n$, and $\langle x^4 \rangle / L^4 = \frac{3}{4}n^2 - \frac{3}{8}n$, which lead to $\kappa_4 / L^4 = -\frac{3}{8}n$ (see Fig. 9 for comparison with simulation). Thus, from Eqs. (21), (33), and (35) one can calculate the cumulants, from which other useful quantities such as the skewness β_1 and kurtosis β_2 measures can be obtained as

$$\begin{aligned} \beta_1 &= \frac{\kappa_3}{\kappa_2^{3/2}} = 0, \\ \beta_2 &= \frac{\kappa_4}{\kappa_2^2} = \frac{\langle x^4 \rangle}{\langle x^2 \rangle^2} - 3. \end{aligned} \tag{36}$$

In Fig. 10, the time evolution of kurtosis is shown for different turning-angle distributions. For a simple random walk, β_2 decreases as $-3/2n$. Moreover, in anomalous diffusive cases, β_2 asymptotically converges to zero since the long-term behavior is diffusion.

It is notable that the higher moments are influenced by the details of the shape of the turning-angle distribution $R(\phi)$. While the MSD depends only on $\mathcal{R} \equiv \mathcal{R}(1)$ (i.e., $\langle \cos\phi \rangle$), $\langle x^4 \rangle$ is a function of both $\mathcal{R}(1)$ and $\mathcal{R}(2)$ (i.e., $\langle \cos\phi \rangle$ and $\langle \cos 2\phi \rangle$). Thus, looking at the behavior of the higher moments would reveal the underlying differences between turning-angle distributions, which are not visible from the MSD results. For example, $\mathcal{R}$ equals to zero for the three different distributions $R(\phi)$ introduced in Fig. 6(a), thus, their MSD is the same. However, their $\mathcal{R}(2)$ is 0, −1, and 1 for $R_1(\phi)$, $R_2(\phi)$, and $R_3(\phi)$, respectively. Therefore, one obtains different analytical expressions for their higher moments such as $\langle x^4 \rangle$.

Besides the components of the displacement, the net distance r of the walker from the origin is also a quantity of interest. For a persistent walk with an arbitrary turning-angle distribution, so far there has been no exact closed-form expression for $\langle r \rangle$. For approximate expressions $\langle r \rangle \approx \sqrt{\langle r^2 \rangle}\left(1 - \frac{1}{8}\frac{\sigma_{r^2}}{\langle r^2 \rangle^2}\right)$ (short-time [13]) and $\langle r \rangle \approx \frac{1}{2}\sqrt{\pi \langle r^2 \rangle}$ (asymptotic [14]), one deals with the calculation of $\langle r^2 \rangle$ and $\langle r^4 \rangle$. The second moment $\langle r^2 \rangle$ can be obtained from Eq. (21) since $\langle r^2 \rangle = \langle x^2 + y^2 \rangle = \langle x^2 \rangle + \langle y^2 \rangle$. The fourth moment reads $\langle r^4 \rangle = \langle (x^2 + y^2)^2 \rangle = \langle x^4 \rangle + 2\langle x^2 y^2 \rangle + \langle y^4 \rangle$. In general, $\langle x^2 y^2 \rangle \neq \langle x^2 \rangle \langle y^2 \rangle$ [see Fig. 11(a)]. In order to calculate $\langle x^2 y^2 \rangle$, one can start from Eq. (3) and follow the analytical procedure as explained for arbitrary moments $\langle x^i \rangle$. For example, a simple random walk with $p = A_1 = A_2 = 0$ and $\lambda = 1$ leads to $\langle x^2 y^2 \rangle = \frac{1}{4}n^2 - \frac{1}{8}n$ versus $\langle x^2 \rangle \langle y^2 \rangle = \frac{1}{4}n^2$. Finally, the analytical form of $\langle r^4 \rangle$ for a walker with constant step size L and isotropic initial conditions is obtained as

$$\langle r^4 \rangle_n = \frac{1}{4}L^4 \Bigg(\frac{(3A_1 + 1)n^2 + (A_1 + 1)(n - 1)n}{1 - A_1} - 4\frac{A_1 A_2 \left[A_2 (A_1 + A_2)\left(A_1 - A_1^{n-1}\right) + (A_2 - A_1)\left(A_2 - A_2^n\right) \right]}{(1 - A_1)(1 - A_2)(A_2 - A_1)^2}$$

$$- 4\frac{A_1 \left(1 - A_1^n\right) n + A_1^2 (3n - n^2) - 2A_1^2 \left(A_1^n + 1\right) + A_1 (n - 1) + 0.5 A_1 (A_1 + 1)(n^2 - n - 2)}{(1 - A_1)^2}$$

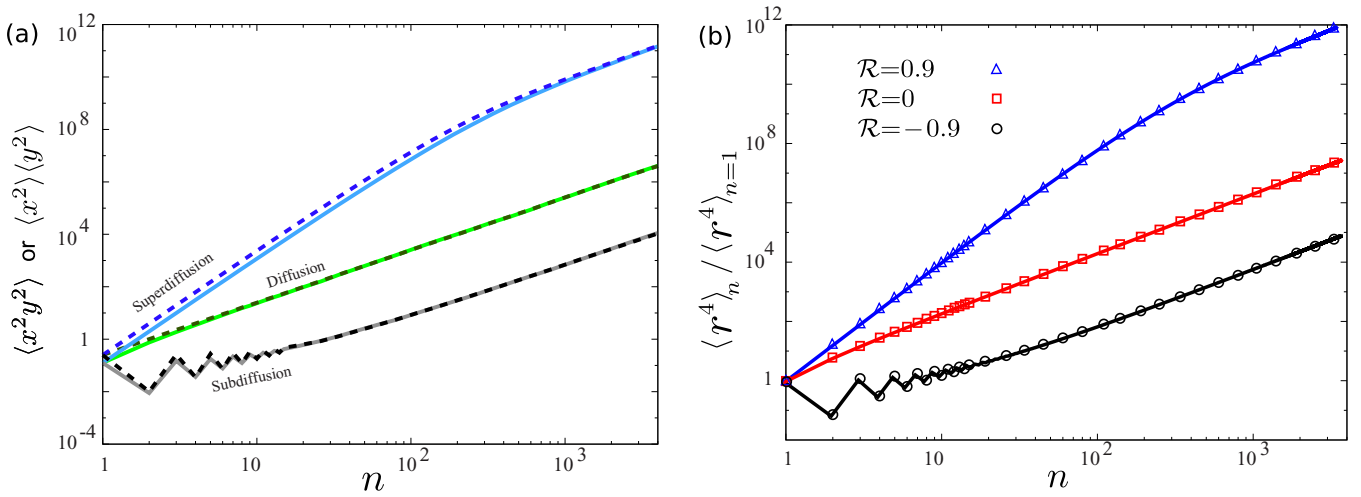

FIG. 11. (Color online) (a) Comparison between $\langle x^2y^2\rangle$ (solid lines) and $\langle x^2\rangle\langle y^2\rangle$ (dashed lines) (both presented in units of $\langle \ell^4\rangle$), obtained from the simulations where the short-time motion is sub- ($\mathcal{R}=-0.9$), normal ($\mathcal{R}=0$), or superdiffusion ($\mathcal{R}=0.9$). (b) $\langle r^4\rangle$ vs n from simulations (symbols) or via Eq. (37) (solid lines).

$$
\begin{aligned}
&+4\frac{-2A_1^{n+2}n+A_1^n+2A_1^4-A_1^3(n^2+3n-9)-A_1^2(n-2)+A_1(n-2)n}{(1-A_1)^3}+\frac{2(A_1+1)A_2(n-1)}{(1-A_1)(1-A_2)}\\
&+4\frac{A_1^2\{A_1[2A_1(A_1+2)+2n-1]-2n+5\}-\left[A_1\left(2A_1^3+4A_1+3\right)+1\right]A_1^n}{(1-A_1)^4}-\frac{2(A_1+1)\left(A_2^2-A_2^{n+1}\right)}{(1-A_1)(1-A_2)^2}\\
&+8\frac{[2A_2-A_1(A_2+1)]\left(A_1^3-A_1^{n+1}\right)n-A_1^3(n-1)[2A_2-A_1(A_2+1)]}{(1-A_1)^3(A_2-A_1)}\\
&-\frac{4A_1A_2(A_1+1)\left[(1-A_1)(n-2)-\left(A_1-A_1^{n-1}\right)\right]}{(1-A_1)^3(A_2-1)}+4\frac{2[2A_2-A_1(A_2+1)]A_1^{n+1}+A_1A_2\left(A_1-A_1^n\right)}{(1-A_1)^2(A_2-A_1)}\\
&+\frac{8A_1[2A_2-A_1(A_2+1)]\left(A_1^3-A_1^{n+2}\right)}{(1-A_1)^4(A_2-A_1)}+\frac{4A_1A_2^2(A_1+A_2)\left(A_2-A_2^{n-1}\right)}{(1-A_2)^2(A_2-A_1)^2}\Bigg),
\end{aligned}
\tag{37}
$$

which is confirmed by the simulation data, as shown in Fig. 11(b). When p is set to zero, Eq. (37) reduces to the expression recently proposed in Ref. [18], even though our formalism allows for obtaining $\langle r^4\rangle$ in the more general case of $p\neq 0$ and even $\lambda\neq 1$ (i.e., variable step lengths) and anisotropic initial conditions. One can similarly calculate the cumulants and relative cumulants such as the kurtosis for the net displacement r. For example, one finds that $-\kappa_4$ grows as n^2+n in the simple case of $p=A_1=A_2=0$, as shown in Fig. 9 (inset).

VI. PROBABILITY DISTRIBUTIONS OF THE NET DISTANCE AND TURNING ANGLE AFTER *n* STEPS

In this section, we show how the probability densities of the position of the random walker and its orientation evolve with time. First, we study the probability distribution $P(r)$ of the distance r of the persistent random walker from the origin in simulations. For a simple random walk in 2D, the shape of the distribution at step n approaches

$$
P(r)\simeq\frac{2r}{\alpha Dn}e^{-\frac{r^2}{\alpha Dn}} \tag{38}
$$

in the large n limit (D is the diffusion constant and $\alpha=4\langle\ell\rangle/v$). However, the anomalous motion of the persistent walker at short times alters the shape of $P(r)$ as well as its propagation speed. In Fig. 12(a), $P(r)$ is plotted at different values of n for $p=0$ and three turning-angle distributions with $\mathcal{R}=-0.9,0$, and 0.9. From Eq. (38) one expects that all normal-diffusion data collapse onto a universal curve when $P(r)\sqrt{n}$ is plotted versus $r/\sqrt{n}$ (see the inset). However, the distributions of sub- and superdiffusion do not follow such a master curve at short times. Indeed, $P(r)$ is narrower and the peak shifts to the left (right) for subdiffusion (superdiffusion) [see Fig. 12(b) (left)]. In the extreme limit of localization or ballistic motion, $P(r)$ will be a δ function at $r=0$ or $r=n\langle\ell\rangle$, respectively. A similar comparison at long times reveals that $P(r)$ broadens slower (faster) than a simple random walk in the case of subdiffusion (superdiffusion). The shapes are, however, expected to follow Eq. (38), as the asymptotic motion is diffusive with different diffusion coefficients obtained from Eq. (19). When scaled by $\sqrt{Dn}$, one finds

$$
P(r)\sqrt{Dn}\simeq\frac{2r}{\alpha\sqrt{Dn}}e^{-\frac{r^2}{\alpha Dn}}, \tag{39}
$$

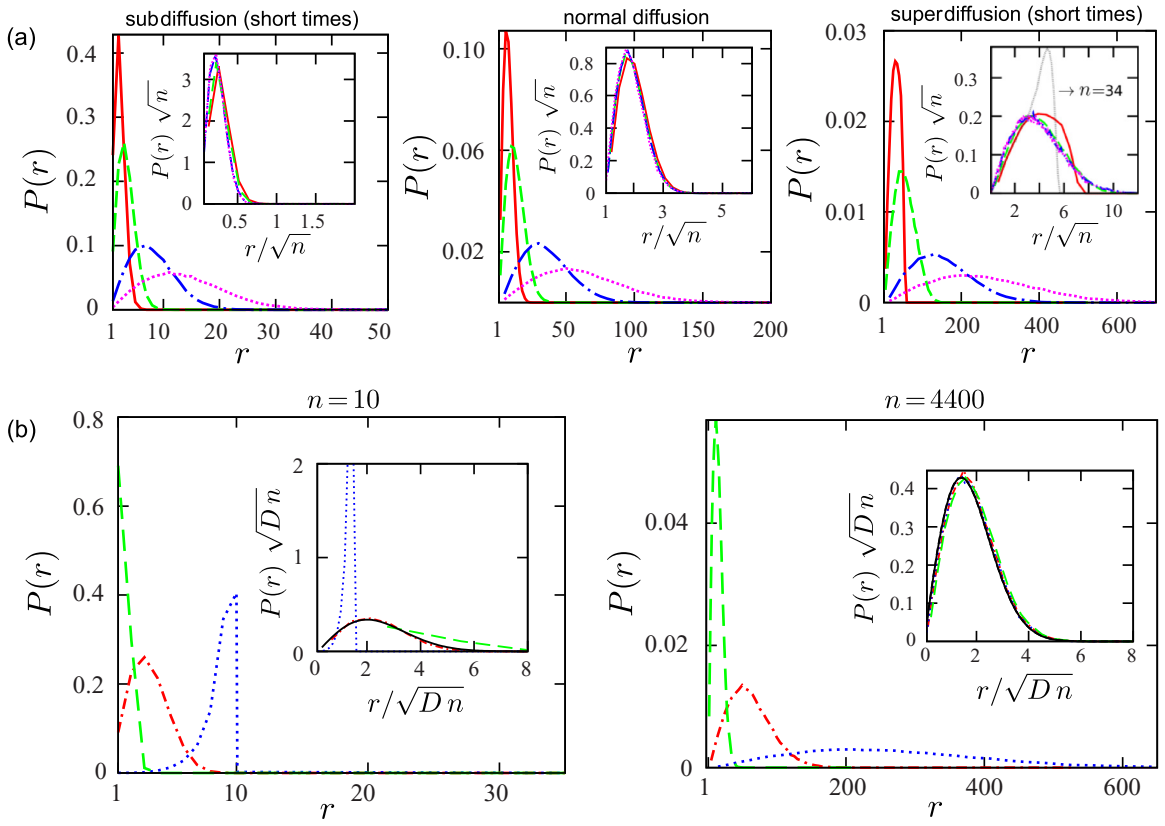

FIG. 12. (Color online) (a) Probability distribution of the distance r (in units of $\langle \ell \rangle$) from the origin at $n = 60, 190, 1400$, and 4400 (solid, dashed, dash-dotted, and dotted lines, respectively), separately shown for persistent walks with short-time sub- (left), normal (middle), and superdiffusive motion (right). Insets: Collapse of $P(r)\sqrt{n}$ vs $r/\sqrt{n}$. (b) Comparison between persistent walks with short-time sub- (dashed lines), normal (dash-dotted lines), and superdiffusive motion (dotted lines) at the early stages of the walk (left) and after a long time (right). Insets: $P(r)\sqrt{Dn}$ in terms of $r/\sqrt{Dn}$, where D is the asymptotic diffusion coefficient. The solid lines are obtained from Eq. (39).

thus, we achieve a data collapse for $P(r)\sqrt{Dn}$ versus $r/\sqrt{Dn}$ in the asymptotic regime of the persistent walks when the motility is purely diffusive, as shown in Fig. 12(b) (right). For random walks in 3D, Eq. (38) should be replaced with $P(r) \simeq \frac{4}{\sqrt{\pi}} \frac{r^2}{(\alpha Dn/2)^{3/2}} e^{-\frac{r^2}{\alpha Dn}}$.

Finally, we investigate how the introduced angular correlations between successive steps weaken over time. This is reflected, e.g., in the evolution of the shape of the probability $f_n(\alpha)$ that the direction of motion after n steps makes an angle α with the current direction of motion. An ordinary random walk is memoryless meaning that the walker gets randomized immediately, thus, $f_n(\alpha)$ remains isotropic over the whole range of time. However, $f_n(\alpha)$ is expected to exhibit anisotropic shapes at short times for persistent walks, with a gradual transition towards isotropic distributions in the limit of large n. Let us consider the case $p = 0$ for simplicity, i.e., the walker turns to a new direction at each step. The probability $f_n(\alpha)$ reads

$$f_n(\alpha) = \int \cdots \int d\phi_1 \cdots d\phi_n \, R(\phi_1) \cdots R(\phi_n) \delta(\phi_1 + \cdots + \phi_n - \alpha), \tag{40}$$

where ϕ_i denotes the turning angle at step i. Using the discrete Fourier transform of the delta function $\delta(x-\alpha) = \frac{1}{2\pi} \sum_{k=-\infty}^{\infty} e^{ik(x-\alpha)}$ one obtains the following expression for the walks which are symmetric with respect to the arrival direction:

$$f_n(\alpha) = \frac{1}{2\pi} \left[1 + 2 \sum_{k=1}^{\infty} \mathcal{R}^n(k) \cos(k\alpha) \right]. \tag{41}$$

In the case of $\alpha = \pm\pi/2$, $f_n(\pm\pi/2)$ reflects the chance of turning to a perpendicular direction after n steps, which can be considered as a measure of the coupling between longitudinal and perpendicular transport. Figure 13 shows that Eq. (41) is in agreement with simulation results.

VII. SUMMARY AND OUTLOOK

A persistent-random-walk model was introduced to study the stochastic motion of self-propelled particles. By developing a general master equation formalism and a Fourier-Z-transform technique it was shown that analytical exact expressions can be obtained for the time evolution of arbitrary moments of displacement. The combination of self-propulsion and characteristics of step-size and turning-angle distributions lead to a rich transport phase diagram at short times. The long-time behavior is, however, diffusive since the successive step angles in the proposed master equation are only indirectly correlated over a few number of steps. This defines a time scale between two arbitrarily chosen steps beyond which

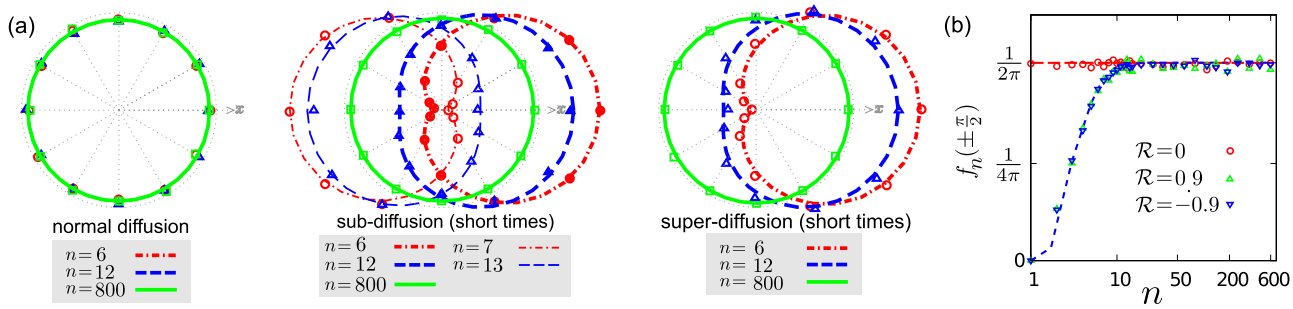

FIG. 13. (Color online) (a) Evolution of the angular distribution $f_n(\alpha)$ of the direction of motion α in the lab frame. The walker initially arrives along the $+x$ direction. A comparison is made between motions with short-time sub- ($\mathcal{R} = -0.9$), normal ($\mathcal{R} = 0$), and superdiffusion ($\mathcal{R} = 0.9$). The lines are obtained from Eq. (41) and symbols denote simulation results. The gray (dotted) lines are guides to eye. (b) Probability $f_n(\pm\frac{\pi}{2})$ of turning to a perpendicular direction after n steps from simulations (symbols) or via Eq. (41) (dashed lines).

the steps are practically independent of each other. It will be interesting to enhance the correlation range, e.g., by introducing (anti-)cross correlations between processivity, step sizes, and turning angles. For particular functional forms of (anti-)cross correlations, one could even obtain a stationary increment for the mean-square displacement (either sub- or superdiffusion) over finite time scales as observed for the motion in viscoelastic environments.

ACKNOWLEDGMENTS

This work was funded by the Deutsche Forschungsgemeinschaft (DFG) through Collaborative Research Centers SFB 1027 (Projects No. A7 and No. A3).

APPENDIX A: ALGEBRAIC COUPLED EQUATIONS FOR THE TAYLOR EXPANSION COEFFICIENTS $Q_i(z,\alpha\,|\,m)$

$$Q_0(z,\alpha\,|\,m) = \frac{z\,Q_{0,n=0}(\alpha\,|\,m)}{z-[p+s\,\mathcal{R}(m)]}, \tag{A1}$$

$$Q_1(z,\alpha\,|\,m) = \frac{z\,Q_{1,n=0}(\alpha\,|\,m)}{z-[p+s\,\mathcal{R}(m)]} + \frac{1}{2}e^{i\alpha}\frac{Q_0(z,\alpha\,|\,m-1)[p+s\,\mathcal{R}(m-1)]}{z-[p+s\,\mathcal{R}(m)]} + \frac{1}{2}e^{-i\alpha}\frac{Q_0(z,\alpha\,|\,m+1)[p+s\,\mathcal{R}(m+1)]}{z-[p+s\,\mathcal{R}(m)]}, \tag{A2}$$

$$\begin{aligned} Q_2(z,\alpha\,|\,m) = {} & \frac{z\,Q_{2,n=0}(\alpha\,|\,m)}{z-[p+s\,\mathcal{R}(m)]} + \frac{1}{2}\frac{Q_0(z,\alpha\,|\,m)[p+s\,\mathcal{R}(m)]}{z-[p+s\,\mathcal{R}(m)]} + \frac{\langle\ell\rangle^2}{\langle\ell^2\rangle}e^{i\alpha}\frac{Q_1(z,\alpha\,|\,m-1)[p+s\,\mathcal{R}(m-1)]}{z-[p+s\,\mathcal{R}(m)]} \\ & + \frac{\langle\ell\rangle^2}{\langle\ell^2\rangle}e^{-i\alpha}\frac{Q_1(z,\alpha\,|\,m+1)[p+s\,\mathcal{R}(m+1)]}{z-[p+s\,\mathcal{R}(m)]} + \frac{1}{4}e^{2i\alpha}\frac{Q_0(z,\alpha\,|\,m-2)[p+s\,\mathcal{R}(m-2)]}{z-[p+s\,\mathcal{R}(m)]} \\ & + \frac{1}{4}e^{-2i\alpha}\frac{Q_0(z,\alpha\,|\,m+2)[p+s\,\mathcal{R}(m+2)]}{z-[p+s\,\mathcal{R}(m)]}, \end{aligned} \tag{A3}$$

$$\begin{aligned} Q_3(z,\alpha\,|\,m) = {} & \frac{z\,Q_{3,n=0}(\alpha\,|\,m)}{z-[p+s\,\mathcal{R}(m)]} + \frac{3}{2}\frac{\langle\ell\rangle\langle\ell^2\rangle}{\langle\ell^3\rangle}\frac{Q_1(z,\alpha\,|\,m)[p+s\,\mathcal{R}(m)]}{z-[p+s\,\mathcal{R}(m)]} \\ & + \frac{3}{8}e^{-i\alpha}\frac{Q_0(z,\alpha\,|\,m+1)[p+s\,\mathcal{R}(m+1)]}{z-[p+s\,\mathcal{R}(m)]} + \frac{3}{8}e^{i\alpha}\frac{Q_0(z,\alpha\,|\,m-1)[p+s\,\mathcal{R}(m-1)]}{z-[p+s\,\mathcal{R}(m)]} \\ & + \frac{1}{8}e^{-3i\alpha}\frac{Q_0(z,\alpha\,|\,m+3)[p+s\,\mathcal{R}(m+3)]}{z-[p+s\,\mathcal{R}(m)]} + \frac{1}{8}e^{3i\alpha}\frac{Q_0(z,\alpha\,|\,m-3)[p+s\,\mathcal{R}(m-3)]}{z-[p+s\,\mathcal{R}(m)]} \\ & + \frac{3}{4}e^{-2i\alpha}\frac{\langle\ell\rangle\langle\ell^2\rangle}{\langle\ell^3\rangle}\frac{Q_1(z,\alpha\,|\,m+2)[p+s\,\mathcal{R}(m+2)]}{z-[p+s\,\mathcal{R}(m)]} + \frac{3}{4}e^{2i\alpha}\frac{\langle\ell\rangle\langle\ell^2\rangle}{\langle\ell^3\rangle}\frac{Q_1(z,\alpha\,|\,m-2)[p+s\,\mathcal{R}(m-2)]}{z-[p+s\,\mathcal{R}(m)]} \\ & + \frac{3}{2}e^{-i\alpha}\frac{\langle\ell\rangle\langle\ell^2\rangle}{\langle\ell^3\rangle}\frac{Q_2(z,\alpha\,|\,m+1)[p+s\,\mathcal{R}(m+1)]}{z-[p+s\,\mathcal{R}(m)]} + \frac{3}{2}e^{i\alpha}\frac{\langle\ell\rangle\langle\ell^2\rangle}{\langle\ell^3\rangle}\frac{Q_2(z,\alpha\,|\,m-1)[p+s\,\mathcal{R}(m-1)]}{z-[p+s\,\mathcal{R}(m)]}, \end{aligned} \tag{A4}$$

$$\begin{aligned} Q_4(z,\alpha\,|\,m) = {} & \frac{z\,Q_{4,n=0}(\alpha\,|\,m)}{z-[p+s\,\mathcal{R}(m)]} + \frac{3}{8}\frac{Q_0(z,\alpha\,|\,m)[p+s\,\mathcal{R}(m)]}{z-[p+s\,\mathcal{R}(m)]} + 3\frac{\langle\ell^2\rangle\langle\ell^2\rangle}{\langle\ell^4\rangle}\frac{Q_2(z,\alpha\,|\,m)[p+s\,\mathcal{R}(m)]}{z-[p+s\,\mathcal{R}(m)]} \\ & + \frac{1}{4}e^{-2i\alpha}\frac{Q_0(z,\alpha\,|\,m+2)[p+s\,\mathcal{R}(m+2)]}{z-[p+s\,\mathcal{R}(m)]} + \frac{1}{4}e^{2i\alpha}\frac{Q_0(z,\alpha\,|\,m-2)[p+s\,\mathcal{R}(m-2)]}{z-[p+s\,\mathcal{R}(m)]} \end{aligned}$$

$$
\begin{aligned}
&+\frac{1}{16}e^{-4i\alpha}\frac{Q_0(z,\alpha\mid m+4)[p+s\,\mathcal{R}(m+4)]}{z-[p+s\,\mathcal{R}(m)]}+\frac{1}{16}e^{4i\alpha}\frac{Q_0(z,\alpha\mid m-4)[p+s\,\mathcal{R}(m-4)]}{z-[p+s\,\mathcal{R}(m)]}\\
&+\frac{3}{2}e^{-i\alpha}\frac{\langle\ell\rangle\langle\ell^3\rangle}{\langle\ell^4\rangle}\frac{Q_1(z,\alpha\mid m+1)[p+s\,\mathcal{R}(m+1)]}{z-[p+s\,\mathcal{R}(m)]}+\frac{3}{2}e^{i\alpha}\frac{\langle\ell\rangle\langle\ell^3\rangle}{\langle\ell^4\rangle}\frac{Q_1(z,\alpha\mid m-1)[p+s\,\mathcal{R}(m-1)]}{z-[p+s\,\mathcal{R}(m)]}\\
&+\frac{1}{2}e^{-3i\alpha}\frac{\langle\ell\rangle\langle\ell^3\rangle}{\langle\ell^4\rangle}\frac{Q_1(z,\alpha\mid m+3)[p+s\,\mathcal{R}(m+3)]}{z-[p+s\,\mathcal{R}(m)]}+\frac{1}{2}e^{3i\alpha}\frac{\langle\ell\rangle\langle\ell^3\rangle}{\langle\ell^4\rangle}\frac{Q_1(z,\alpha\mid m-3)(p+s\,\mathcal{R}(m-3))}{z-(p+s\,\mathcal{R}(m))}\\
&+\frac{3}{2}e^{-2i\alpha}\frac{\langle\ell^2\rangle\langle\ell^2\rangle}{\langle\ell^4\rangle}\frac{Q_2(z,\alpha\mid m+2)[p+s\,\mathcal{R}(m+2)]}{z-[p+s\,\mathcal{R}(m)]}+\frac{3}{2}e^{2i\alpha}\frac{\langle\ell^2\rangle\langle\ell^2\rangle}{\langle\ell^4\rangle}\frac{Q_2(z,\alpha\mid m-2)[p+s\,\mathcal{R}(m-2)]}{z-[p+s\,\mathcal{R}(m)]}\\
&+2e^{-i\alpha}\frac{\langle\ell\rangle\langle\ell^3\rangle}{\langle\ell^4\rangle}\frac{Q_3(z,\alpha\mid m+1)[p+s\,\mathcal{R}(m+1)]}{z-[p+s\,\mathcal{R}(m)]}+2e^{i\alpha}\frac{\langle\ell\rangle\langle\ell^3\rangle}{\langle\ell^4\rangle}\frac{Q_3(z,\alpha\mid m-1)[p+s\,\mathcal{R}(m-1)]}{z-[p+s\,\mathcal{R}(m)]}. \qquad \text{(A5)}
\end{aligned}
$$

APPENDIX B: THE FIRST TWO MOMENTS OF DISPLACEMENT IN THE z SPACE

$$
\langle x\rangle(z)=\sum_{n=0}^{\infty}z^{-n}\langle x\rangle_n=\frac{z}{z-1}\langle\ell\rangle\,Q_{1,n=0}(0\mid 0)+\frac{z}{z-1}\frac{\langle\ell\rangle}{2}\frac{Q_{0,n=0}(0\mid -1)A_{-1}}{z-A_{-1}}+\frac{z}{z-1}\frac{\langle\ell\rangle}{2}\frac{Q_{0,n=0}(0\mid 1)A_{1}}{z-A_{1}}, \qquad \text{(B1)}
$$

$$
\begin{aligned}
\langle x^2\rangle(z)=\sum_{n=0}^{\infty}z^{-n}\langle x^2\rangle_n&=\frac{z}{z-1}\langle\ell^2\rangle Q_{2,n=0}(0\mid 0)+\frac{z}{(z-1)^2}\frac{\langle\ell^2\rangle}{2}Q_{0,n=0}(0\mid 0)\\
&+\frac{z}{z-1}\langle\ell\rangle^2\left[\frac{Q_{1,n=0}(0\mid 1)\,A_1}{(z-A_1)}+\frac{Q_{1,n=0}(0\mid -1)\,A_{-1}}{(z-A_{-1})}\right]+\frac{z}{(z-1)^2}\frac{\langle\ell\rangle^2}{2}\left[\frac{Q_{0,n=0}(0\mid 0)\,A_1}{(z-A_1)}+\frac{Q_{0,n=0}(0\mid 0)\,A_{-1}}{(z-A_{-1})}\right]\\
&+\frac{z}{z-1}\frac{\langle\ell\rangle^2}{2}\left[\frac{Q_{0,n=0}(0\mid 2)\,A_1\,A_2}{(z-A_1)(z-A_2)}+\frac{Q_{0,n=0}(0\mid -2)\,A_{-1}\,A_{-2}}{(z-A_{-1})(z-A_{-2})}\right]\\
&+\frac{z}{z-1}\frac{\langle\ell^2\rangle}{4}\left[\frac{Q_{0,n=0}(0\mid 2)A_2}{(z-A_2)}+\frac{Q_{0,n=0}(0\mid -2)A_{-2}}{(z-A_{-2})}\right]. \qquad \text{(B2)}
\end{aligned}
$$

[1] J. L. Ross, M. Y. Ali, and D. M. Warshaw, Curr. Opin. Cell Biol. **20**, 41 (2008).

[2] J. R. Howse, R. A. L. Jones, A. J. Ryan, T. Gough, R. Vafabakhsh, and R. Golestanian, Phys. Rev. Lett. **99**, 048102 (2007).

[3] F. Peruani and L. G. Morelli, Phys. Rev. Lett. **99**, 010602 (2007).

[4] M. R. Shaebani, Z. Sadjadi, I. M. Sokolov, H. Rieger, and L. Santen, Phys. Rev. E **90**, 030701(R) (2014).

[5] R. Nossal and G. H. Weiss, J. Theor. Biol. **47**, 103 (1974); P. M. Kareiva and N. Shigesada, Oecologia **56**, 234 (1983).

[6] E. A. Codling, M. J. Plank, and S. Benhamou, J. R. Soc. Interface **5**, 813 (2008).

[7] B. B. Mandelbrot and J. W. Van Ness, SIAM Rev. **10**, 422 (1968); E. Lutz, Phys. Rev. E **64**, 051106 (2001).

[8] B. D. Hughes, *Random Walks and Random Environments* (Clarendon, Oxford, 1995), Vol. 1; R. Metzler and J. Klafter, Phys. Rep. **339**, 1 (2000).

[9] P. C. Bressloff and J. M. Newby, Rev. Mod. Phys. **85**, 135 (2013); F. Höfling and T. Franosch, Rep. Prog. Phys. **76**, 046602 (2013).

[10] M. Y. Ali *et al.*, Proc. Natl. Acad. Sci. USA **104**, 4332 (2007); K. Shiroguchi and K. Kinosita, Science **316**, 1208 (2007).

[11] M. Vershinin *et al.*, Proc. Natl. Acad. Sci. USA **104**, 87 (2007).

[12] Y. Okada, H. Higuchi, and N. Hirokawa, Nature **424**, 574 (2003); T. L. Culver-Hanlon *et al.*, Nat. Cell Biol. **8**, 264 (2006).

[13] C. E. McCulloch and M. L. Cain, Ecology **70**, 383 (1989).

[14] P. Bovet and S. Benhamou, J. Theor. Biol. **131**, 419 (1988).

[15] M.-F. Miri and H. Stark, J. Phys. A **38**, 3743 (2005); Z. Sadjadi and M.-F. Miri, Phys. Rev. E **84**, 051305 (2011); Z. Sadjadi, M. F. Miri, M. R. Shaebani, and S. Nakhaee, *ibid.* **78**, 031121 (2008).

[16] M. R. Shaebani, J. Sarabadani, and D. E. Wolf, Phys. Rev. Lett. **108**, 198001 (2012); Phys. Rev. E **88**, 022202 (2013); A. Kudrolli, G. Lumay, D. Volfson, and L. S. Tsimring, Phys. Rev. Lett. **100**, 058001 (2008).

[17] P. de Anna, T. Le Borgne, M. Dentz, A. M. Tartakovsky, D. Bolster, and P. Davy, Phys. Rev. Lett. **110**, 184502 (2013).

[18] A. Cheung, J. Theor. Biol. **264**, 641 (2010).